Entropy and Seebeck signals meet on the edges

Natalia Cortés,[1,2,*] Patricio Vargas,[3] and S. E. Ulloa[2]

[1]*Instituto de Alta Investigación, Universidad de Tarapacá, Casilla 7D, Arica, Chile*

[2]*Department of Physics and Astronomy, and Nanoscale and Quantum Phenomena Institute, Ohio University, Athens, Ohio 45701-2979, USA*

[3]*Departamento de Física, CEDENNA, Universidad Técnica Federico Santa María, Casilla 110V, Valparaíso, Chile*

(Received 30 September 2022; revised 21 December 2022; accepted 14 February 2023; published 23 February 2023)

We explore the electronic entropy per particle s and Seebeck coefficient $\mathcal{S}$ in zigzag graphene ribbons. Pristine and edge-doped ribbons are considered using tight-binding models to inspect the role of edge states in the observed thermal transport properties. As a band gap opens when the ribbons are doped at one or both edges, due to asymmetric edge potentials, we find that s and $\mathcal{S}$ signals are closely related to each other: both develop sharp dip-peak line shapes as the chemical potential lies in the gap, while the ratio $s/\mathcal{S}$ exhibits a near-constant value equal to the elementary charge e at low temperatures. This constant ratio suggests that $\mathcal{S}$ can be seen as the transport differential entropy per charge, as suggested by some authors. Our calculations also indicate that measurement of s and $\mathcal{S}$ may be useful as a spectroscopic probe of different electronic energy scales involved in such quantities in gapped materials.

DOI: 10.1103/PhysRevB.107.075433

I. INTRODUCTION

Nearly forty years ago, Rockwood argued that the thermoelectric power (TEP) or Seebeck coefficient $\mathcal{S}$ in any material is proportional to the total electronic entropy S as $\mathcal{S} = -S/F$ with F the Faraday constant [1]. Another relation, the Kelvin formula, connects the TEP with the charge carrier number N derivative of S at constant temperature T, $\mathcal{S}_K = (1/e)(\partial S/\partial N)_T$ [2]. It has also been shown that $\mathcal{S} \sim \mathcal{S}_K$ holds qualitatively for noninteracting electrons in a single band (simple metal), in strongly correlated systems [3,4], as well as in the incoherent metal regime in ruthenates [5]. Several authors have further analyzed the entropy per particle $s = (\partial S/\partial N)_T$ to provide a fundamental characterization of the thermodynamics of electronic states in different material systems [6–13].

The TEP $\mathcal{S}$ is defined as the voltage gradient response ΔV to a temperature gradient ΔT at vanishing electric current flux, $\mathcal{S} = \Delta V/\Delta T|_{I=0}$ [5]. $\mathcal{S}$ can be obtained from electronic transport calculations and experiments, revealing characteristic line shapes as function of gate voltage or chemical potential μ, probing particle-hole asymmetries in the systems [3]. On graphene-based samples, $\mathcal{S}$ exhibits peak-dip line shapes given by the contribution of electrons and holes as a gate voltage or μ changes. For example, in monolayer graphene, a dip-peak curve is seen near the charge neutrality point, broadening its features with increasing temperature [14]. For gated bilayer graphene systems, the dip-peak shape appears inside the band gap of the band structure [15,16], and enhanced dip-peak magnitudes are seen when graphene ribbon samples are patterned with defined edges [17,18].

Thermodynamic measurements of the total entropy S (notice $s \neq S$ [6]) have allowed the acquisition of fundamental information about the electronic state of quantum dots [19], magic angle twisted bilayer graphene systems [20,21], and even a universal value in disordered zigzag graphene ribbons [22]. Similar analysis of the total entropy S has been carried out in metals and other systems at high temperatures [23], as well as electrons in disordered materials [24]. The entropy per particle s provides an excellent thermodynamic tool, exhibiting high sensitivity in low charge density regimes, with experimental evidence of dip-peak curves showing zeros near even filling factors [25]. Theoretical results for $s(\mu)$ show that it exhibits peak-dip structures in diverse 2D materials, including gapped graphene monolayers [8], semiconducting dichalcogenides [10], and gated germanene [9]. Although s is not a transport quantity, it can display line shapes similar to those of $\mathcal{S}$, suggesting a close interconnection between both quantities not yet explored in 2D materials. We are interested in how these quantities may reflect the spectral features of the system and whether they exhibit similar characteristics in order to fulfill the transport of s as $\mathcal{S} = s/e$ as a function of chemical potential and temperature.

To explore the connection between s and $\mathcal{S}$, we consider edge-doped zigzag graphene ribbons with different widths. The selection of these systems allows us to analyze how the flat bands near the charge neutrality point (zero energy) [26,27], and gapped states when the ribbons are doped on the edges [28,29], behave as s and $\mathcal{S}$ are obtained at low and relatively high temperatures [30]. We find the flat bands for zigzag edges are captured by a peak-dip signal in s, similar to that produced by the flat state in Lieb's square lattice [13]. Such flat bands result in vanishing $\mathcal{S}$ values for pristine ribbons but transform into $\mathcal{S} = -2\frac{k_B}{e}\ln 2$ right at the edge state in gapped ribbons. Most interestingly, a near proportionality $s \propto \mathcal{S}$

*nc747821@ohio.edu

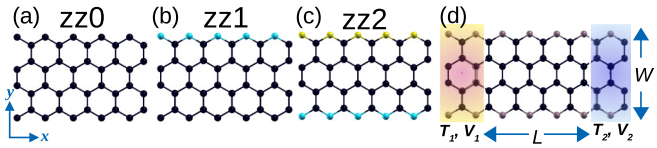

FIG. 1. Undoped and doped simulated zigzag graphene ribbons. (a) Pristine undoped zz0, (b) top edge doped zz1, (c) both edges doped zz2. (d) Each ribbon is connected to two leads, held at voltage V_1 and temperature T_1 on the left and V_2, T_2 on the right side. Ribbon size and shape are schematic with length L, width W, and zigzag edges along the x axis. Black spheres represent carbon atoms with on-site energy $\delta_0 = 0$, cyan spheres in (b) and (c) stand for edge atoms with on-site energy of $\delta_1 = 0.2\,\text{eV}$, and yellow spheres in (c) indicate top on-site energies of $\delta_2 = -0.4\,\text{eV}$.

occurs inside the band gap of doped ribbons, both appearing as sharp peak-dip curves. We in fact find that the ratio $s/\mathcal{S}$ has a nearly constant value of e as μ shifts within the gap at low T, except for a narrow discontinuity around the gap midpoint. We then confirm the near equality $\mathcal{S} \simeq s/e$, demonstrating the Kelvin formula and the relation argued early by Rockwood [31]. The relation $s/\mathcal{S} \simeq e$ is expected to be valid for other gapped electronic systems, and their strong sensitivity to gaps and van Hove singularities can be used as practical probes of the electronic structure. This relation suggests further that the TEP can be seen as the transported entropy per charge, providing an interesting connection between a transport quantity and a thermodynamic measure.

II. MODEL

To describe the low-energy spectrum in pristine and edge-doped zigzag graphene ribbons, we use π-orbital tight-binding models constructed in real space with the PYBINDING code [32]. For pristine ribbons [labeled as zz0 in Fig. 1(a)], we fix the on-site energies throughout at zero $\delta_0 = 0$. Edge-doped ribbons are modeled by changing the on-site potentials on the edges to simulate gapped systems, as seen for example in edge-oxidized and edge-nitrided doped ribbons [29]. In a single-edge-doped ribbon [zz1 in Fig. 1(b)], the atoms at the top edge have on-site energy $\delta_1 = 0.2\,\text{eV}$. For both doped edges (zz2 ribbons), the on-site energies at the top edge are $\delta_2 = -0.4\,\text{eV}$, and δ_1 at the bottom edge, Fig. 1(c). This allows us to inspect the role that edge states as well as gapped states have on the thermal transport and thermodynamic response, which we will see is quite important, as s and $\mathcal{S}$ can show (non)equivalent signals as T and μ change.

With the dispersion relation results for each ribbon system, we calculate the ribbon density of states (DoS), D, counting states along the k_x-momentum path $X' - K - \Gamma - K' - X$. The ribbons are then connected to extended pristine graphene ribbon current leads to obtain the charge transport characteristics (transmission probability τ) using the KWANT code [33]. The leads at the ribbon left and right are held at a voltage difference $\Delta V = V_1 - V_2 > 0$, and consider the linear response regime, i.e., $|e\Delta V| \ll \mu$, where μ is the overall chemical potential. To obtain the TEP response, we consider a temperature gradient ΔT between the leads with $\Delta T = T_1 - T_2 > 0$, as illustrated in Fig. 1(d). The TEP is quantified by the Seebeck coefficient $\mathcal{S}$, which can be expressed in terms of the thermal integrals $L_n = \frac{2}{h}\int_{-\infty}^{\infty} \tau(\varepsilon)(\varepsilon-\mu)^n(-\frac{\partial f}{\partial \varepsilon})d\varepsilon$, as [34]

$$\mathcal{S} = \frac{1}{eT}\frac{L_1}{L_0} = \frac{k_B}{e}\frac{\int_{-\infty}^{\infty}\tau(\varepsilon)\alpha(\varepsilon)\cosh^{-2}\left(\frac{\alpha(\varepsilon)}{2}\right)d\varepsilon}{\int_{-\infty}^{\infty}\tau(\varepsilon)\cosh^{-2}\left(\frac{\alpha(\varepsilon)}{2}\right)d\varepsilon}, \quad (1)$$

where h is the Planck constant, k_B the Boltzmann constant, ε the energy eigenvalues for each system, $f(\varepsilon, T, \mu) = 1/[e^{\beta(\varepsilon-\mu)} + 1]$ the Fermi-Dirac distribution with $\beta = 1/k_BT$, $\tau(\varepsilon)$ the transmission probability function, and $\alpha(\varepsilon) = (\varepsilon - \mu)/k_BT$. Similarly, the entropy per particle s can be expressed as [9,11,12]

$$s = k_B\frac{\int_{-\infty}^{\infty} D(\varepsilon)\alpha(\varepsilon)\cosh^{-2}\left(\frac{\alpha(\varepsilon)}{2}\right)d\varepsilon}{\int_{-\infty}^{\infty} D(\varepsilon)\cosh^{-2}\left(\frac{\alpha(\varepsilon)}{2}\right)d\varepsilon}. \quad (2)$$

Note the similarity of Eqs. (1) and (2), considering that by obtaining $\tau(\varepsilon)$ and $D(\varepsilon)$ respectively, one can capture the equivalence and/or difference between $\mathcal{S}$ and s, providing an efficient and reliable approach to study thermally activated electronic signals in diverse quantum materials, such as gapped graphene ribbons.

III. RESULTS AND DISCUSSION

We compare graphene ribbons zz1 and zz2 with different sizes and contrast their response with that of pristine ribbons zz0. We look at ribbons with a nominal length $L = 8$ nm; L is large enough to consider these results valid for any mesoscopic ribbon. Most relevant characteristic is the ribbon width, as it determines the spacings of the bulk subbands and associated DoS features. The three ribbon widths considered are $W = 2$ nm, $W = 8$ nm, and $W = 12$ nm, which we label $L8W2$, $L8W8$, and $L8W12$, respectively.

It is well known that pristine zigzag ribbons are metallic, regardless of the width, with flat bands at zero energy, Figs. 2(a) and 2(b) [35], due to extended states along both ribbon edges. Edge-atom doping changes that, opening a gap at the charge neutrality point. Figures 2(c) and 2(d) show the band structure, D, and τ for a zz1-$L8W2$ ribbon, while panels (e) and (f) are for the wider ribbon zz1-$L8W8$. Both ribbons exhibit gaps with a magnitude of $\delta_1 = 0.2\,\text{eV}$ at the X, X' points, and smaller gaps near the K, K' points of $\simeq 0.11\,\text{eV}$ for $L8W2$, and $\simeq 0.04\,\text{eV}$ for $L8W8$. The energy gaps near K, K' decrease as the ribbon width increases and the two edges further decouple [36]. The gaps at X, X' open because of the asymmetric on-site potentials on the bottom ($\delta_0 = 0$) and top (δ_1) ribbon edges, which break inversion symmetry in the ribbon. The top valence band shows a zero-energy flat band within the (X', K) and (K', X) windows, associated with the unperturbed bottom edge [35]. The corresponding DoS shows a large peak around zero energy, for both ribbon widths. The gap opening near K, K' results in a parabolic bottom conduction band with local inverted curvature at the X, X' points. These characteristics result in large van Hove singularities (vHs's) in the DoS at the energies of the bottom conduction and inverted bands. Additional van Hove peaks at higher (and lower) energies are due to the onset of bulk subbands, as those shown for $L8W8$ in panels (e) and (f), at energies $\simeq \pm 0.32\,\text{eV}$. These bulk states at larger energies

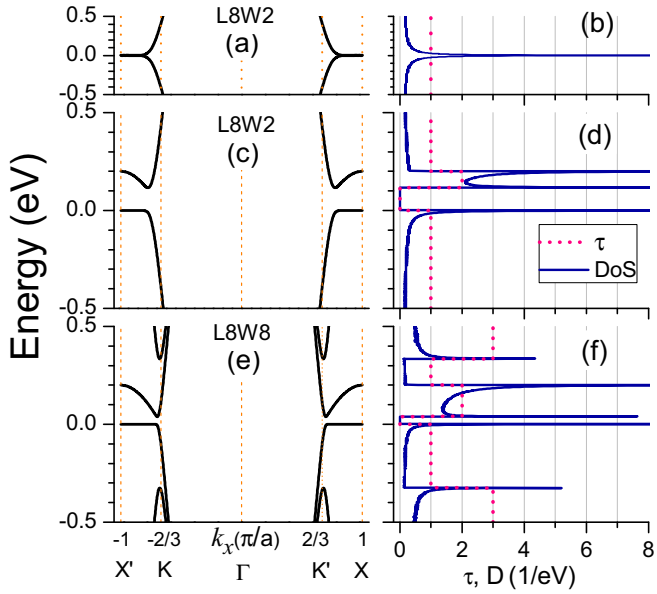

FIG. 2. Electronic spectra for pristine ribbon zz0-$L8W2$ [(a), (b)]; ribbon zz1-$L8W2$ [(c), (d)]; and ribbon zz1-$L8W8$ [(e), (f)]. Left panels show band structure along $X' - K - \Gamma - K' - X$; right panels show transmission τ and density of states D. Numbers along the horizontal axis indicate high-symmetry k_x values, highlighted with orange vertical lines in (a), (c), and (e). Gray vertical lines in (b), (d), and (f) indicate integer steps for τ.

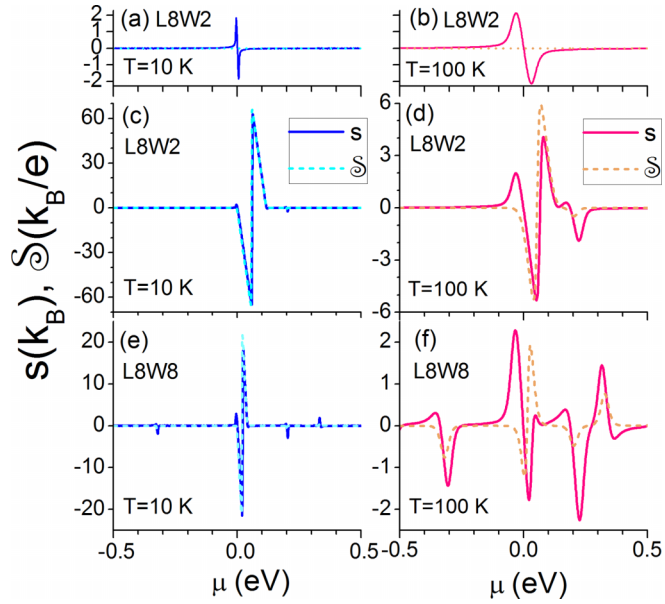

FIG. 3. Entropy per particle s (solid lines) and Seebeck signal $\mathcal{S}$ (dashed lines) for zz0 [(a), (b)] and zz1 ribbons [(c)–(f)]. (a)–(d) Narrow ribbon, $L8W2$; (e), (f) wide ribbon, $L8W8$. Left panels, $T = 10$ K; right panels, $T = 100$ K. Notice different vertical scales for zz1 ribbons.

are common for pristine and doped ribbons [35]. The DoS naturally vanishes for energies within the band gap near the K, K' points. The gaps and van Hove peaks in the DoS will be shown to produce strong signatures in the entropy per particle response, as anticipated from Eq. (2).

When ΔV is turned on at $\Delta T = 0$, charge carriers can be transported along with allowed zigzag channels in the ribbon system with probability $\tau(\varepsilon)$. As a channel opens, τ jumps by 1, as we assume the current leads are pristine graphene ribbons, resulting in the steplike curves seen in Figs. 2, 4, 6. In Figs. 2(d) and 2(f), $\tau(\varepsilon)$ (dotted pink lines) jumps from 1 to 0 at the top valence energy, vanishes in the energy gap, and jumps from 0 to 2 to 1 near the bottom of the conduction band. This quantized electronic transport in ribbons is directly linked to $\mathcal{S}$ via Eq. (1). When the ribbons are placed in a temperature gradient ΔT, the charge carriers are thermally excited and move from the hottest to the coldest lead and vice versa.

In Fig. 3 we present $\mathcal{S}$ (dashed) and s (solid lines) signals as function of μ at $T = 10$ and 100 K for pristine zz0-$L8W2$ and different width zz1 ribbons. The μ scan can be implemented by gate voltages, which would produce corresponding charge density changes in the system [16]. The pristine ribbon shows an antisymmetric response for s around the flat band ($\mu = 0$) while $\mathcal{S}$ vanishes regardless the value of T, Figs. 3(a) and 3(b). When ribbons are doped, $\mathcal{S}$ turns on for each ribbon, and at low temperatures, $T = 10$ K, s and $\mathcal{S}$ exhibit a dip-peak structure with nearly identical shape and amplitude within the energy gap of each ribbon zz1, Figs. 3(c) and 3(e). The shapes are sharper for zz1-$L8W8$ as the electronic structure [Fig. 2(e)] shows a narrower gap for wider ribbons. The large discontinuous sign change for both s and $\mathcal{S}$ occurs near the gap midpoint $\mu_{\rm gmp}$, as the contributions from charge carrier densities (electrons and holes) cancel each other at this $\mu_{\rm gmp}$ value. The similarity $s \simeq \mathcal{S}$ whenever μ crosses the gap comes from the vanishing of the relevant quantity, $\tau(\varepsilon) = D(\varepsilon) = 0$ in this region, making Eqs. (1) and (2) equivalent. As T increases to 100 K, Figs. 3(d) and 3(f), s and $\mathcal{S}$ decrease by one order of magnitude, broaden their shape, and are no longer similar for ribbons $W > 2$ nm. Much higher T destroys the s, $\mathcal{S}$ equivalence [35].

Interestingly, the presence of the flat edge state and its associated sharp DoS are captured by a positive peak in s at $\mu \simeq 0$, decreasing only slightly with T. In contrast, $\mathcal{S}(\mu = 0)$ has a finite value $= -2\frac{k_B}{e} \ln 2$ at low temperatures ($\lesssim 100$ K) for both ribbon widths, as expected from an analytical estimate that sets τ as a Heaviside function [35]. The (inverted) parabolic band edge at $\varepsilon = 0.2$ eV is seen in both s and $\mathcal{S}$ as a negative peak near $\mu = 0.2$ eV, with larger amplitude for s, that decreases with T. The flat and parabolic s and $\mathcal{S}$ edge responses will be discussed in more detail below. As μ shifts away from the gap edges for $L8W8$ in Figs. 3(e) and 3(f), bulk subband features appear in s and $\mathcal{S}$, with s showing a sign change near each DoS maximum. The peaks in $\mathcal{S}$ are positive for electrons and negative for holes; such sign reversal is clear in Fig. 3(d) for $\mu \sim \pm 0.3$ eV. Similar behavior for s and $\mathcal{S}$ at larger μ values is also present for bulk subbands in pristine ribbons [35]. One could use such sign reversal in $\mathcal{S}(\mu)$ to monitor subband curvature changes, as external fields (e.g., strains or voltages) may produce band inversions [37].

For a wider zz1 ribbon $L8W12$, the band structure, DoS, and τ are shown in Fig. 4. In Fig. 4(a), the zz1-$L8W12$ ribbon presents a narrow gap of $\simeq 0.027$ eV near the K, K' points, and a local gap of 0.2 eV at X, X' points is obtained as in

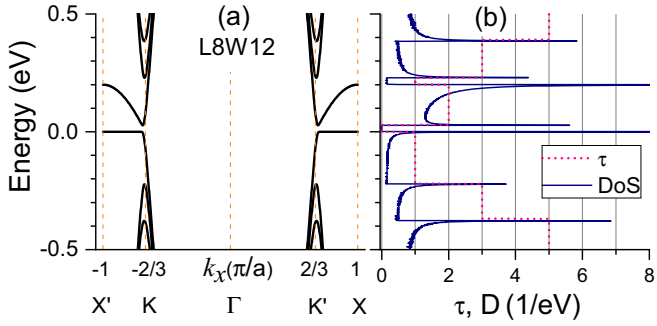

FIG. 4. Electronic spectra for zz1-$L8W12$ ribbon. (a) $X' - K - \Gamma - K' - X$ band structure, (b) transmission τ and density of states D.

the narrow ribbons $L8W2$ and $L8W8$ [2(c), 2(e)]. The band structure shows more bulk subbands at closer energies from the flat band at zero energy (compared to the zz1-$L8W8$ ribbon), as there are more allowed zigzag channels. In Fig. 4(b), the DoS shows a large vHs for the flat band as well as for the parabolic edge state at 0.2 eV; a smaller vHs is seen for the inverted parabolic band at $\simeq 27$ meV, and also for each bulk subband as expected. Similarly to the narrow ribbons, the transmission exhibits the expected jumps at the energy values of the flat band, inverted and parabolic bands, and for each bulk subband vHs.

Figure 5 presents s and $\mathcal{S}$ for zz1-$L8W12$ ribbon. In panel (a), both quantities show high correlation at $T = 10$ K, except for the flat band near $\mu = 0$, comparable to the zz1-$L8W2$ and zz1-$L8W8$ ribbons shown in Figs. 3(c) and 3(e). However, a clear difference occurs here for the zz1-$L8W12$ ribbon compared to zz1 narrower ribbons, as the first conduction bulk subband is at nearly the same energy as the parabolic edge state around $\mu = 0.2$ eV [see Fig. 4(a)]. Consequently, both s and $\mathcal{S}$ at $T = 10$ K have a mix behavior around 0.2 eV, showing a negative peak followed by a positive peak as $|\mu|$ increases, with larger magnitude for s. In Fig. 5(b), s and $\mathcal{S}$ at $T = 100$ K lose their interconnection, especially inside the band gap and at the parabolic state around the region $0 \lesssim \mu \lesssim 0.3$ eV.

Another interesting case is when both zigzag edges are asymmetrically doped, as in the zz2 ribbons in Fig. 1(c). This

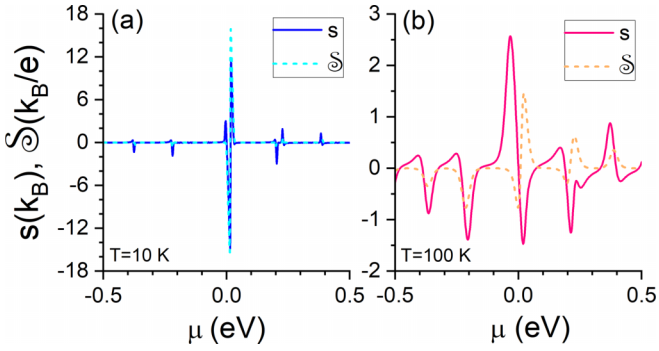

FIG. 5. Entropy per particle s (solid lines) and Seebeck signal $\mathcal{S}$ (dashed lines) for zz1-$L8W12$ ribbon. (a) $T = 10$ K, (b) $T = 100$ K. Notice different vertical scales.

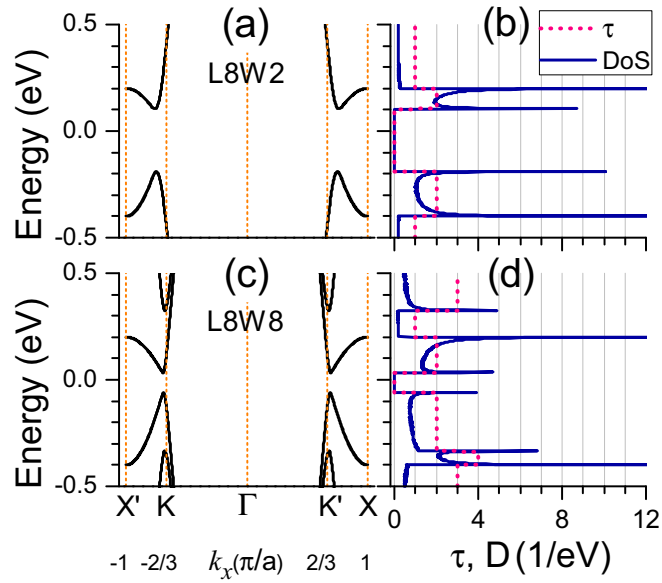

FIG. 6. Electronic spectra for zz2 ribbons. Top row $L8W2$, bottom $L8W8$. (a), (c) $X' - K - \Gamma - K' - X$ band structure; (b), (d) transmission τ and density of states D.

system is similar to ribbons with hydrogen-oxygen doped edges [29], or to a nonmagnetic version of ribbons with antiferromagnetic edges [36,38], [39]. Figure 6 shows the electronic dispersion, DoS, and τ for $L8W2$ and $L8W8$ zz2 systems. The gaps are larger than for zz1 ribbons, as the on-site potentials on the edges contribute additively, producing 0.6 eV gaps at X, X'. Near K, K' the gaps narrow to $\simeq 0.3$ eV for $L8W2$ and $\simeq 0.1$ eV for $L8W8$. We notice there is no flat edge state around zero energy as in zz1 or pristine ribbons. Instead, there is an asymmetric gap about $\varepsilon = 0$, and the edge dispersions are parabolic. The structure is otherwise similar to the case shown in Fig. 2, with rescaled energies: τ and D present similar structure to the zz1 devices but with larger band gaps. As a consequence, the dip-peak structure for s and $\mathcal{S}$ in Fig. 7 is nearly identical within the gaps, with $s \simeq e\mathcal{S}$ at both 10 K and 100 K. The vanishing DoS on both ribbon gap edges results in even more symmetric responses in s and $\mathcal{S}$ for zz2 systems.

We now turn our attention to the electronic-thermodynamic states of zz1 ribbon systems as their dispersions present a flat band at the valence gap edge and a parabolic band at the conduction gap edge. Figure 8(a) clearly exhibits the dip-peak shapes of s and $\mathcal{S}$ within the gap at $T = 10$ K (region highlighted in yellow) for the zz1-$L8W2$ ribbon; the small mismatch near midgap is related to the asymmetric shape of the DoS (dot-dashed black line), especially around the flat band near $\mu = 0$. The area inside the red rectangle focuses on s and $\mathcal{S}$ near the flat band, as shown amplified in the bottom inset. s (blue solid line) presents a positive peak of height $s \sim 3k_B \ln 2$ for negative μ, changes sign near $\mu = 0$ where D has a maximum, and then continues with a constant slope for positive μ [35]. The inset also shows s for the flat band of the pristine ribbon (thin magenta line) with an antisymmetric shape around $\mu = 0$ with peak values of $s \sim \pm 3k_B \ln 2$ [35,40]. In contrast, $\mathcal{S}$ (dashed cyan line) drops monotonically

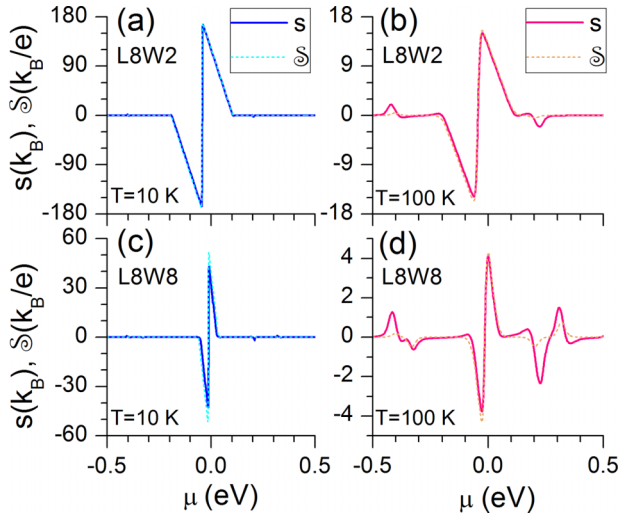

FIG. 7. Entropy per particle s (solid lines) and Seebeck signal $\mathcal{S}$ (dashed lines) for zz2 ribbons. Top row $L8W2$, bottom row $L8W8$. (a), (c) $T = 10$ K; (b), (d) $T = 100$ K. Notice different vertical scales.

at the gap edge, reaches a value $\mathcal{S}(\mu = 0) = -2\frac{k_B}{e}\ln 2$, before having a constant slope for $\mu \lesssim \mu_{\rm gmp}$ [35].

The parabolic band edges at X, X' produce features at $\mu \simeq 0.2$ eV, as displayed in the top inset. The associated van Hove peak in D produces a sign change in s with peak value $\sim -3k_B \ln 2$, whereas $\mathcal{S}$ has a negative peak of height $\mathcal{S} \simeq -0.46\, k_B/e$, its sign indicating the inverted parabolic dispersion. Approximate results for s, $\mathcal{S}$ arising from edge and bulk states can also be described by Sommerfeld expansions for different L_n integrals [35], which agree with these results.

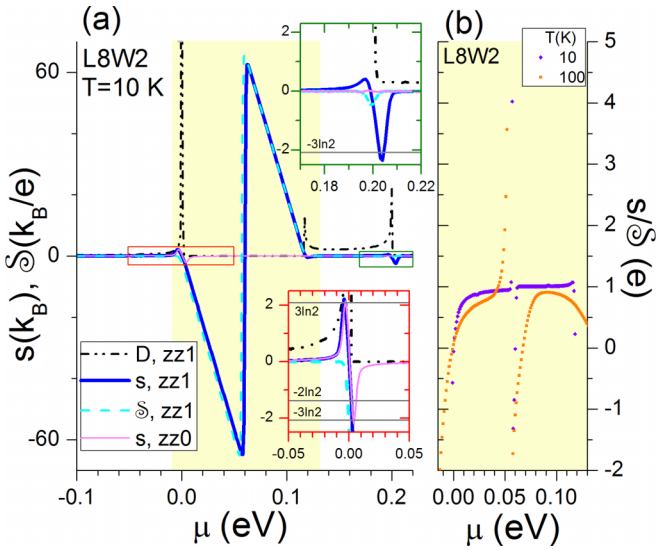

FIG. 8. (a) Entropy per particle $s(\mu)$ (solid blue) and Seebeck signal $\mathcal{S}(\mu)$ (dashed cyan line) at $T = 10$ K for zz1-$L8W2$ ribbon. Dash-dotted black line is the density of states D; solid magenta line shows s for the pristine zz0-$L8W2$ ribbon. Red (green) rectangle indicates areas near the edge states at $\mu = 0$ ($\mu = 0.2$ eV) in the bottom (top) inset. (b) Ratio $s(\mu)/\mathcal{S}(\mu)$ in units of e for curves within the yellow rectangle in (a); results for $T = 100$ K are also included.

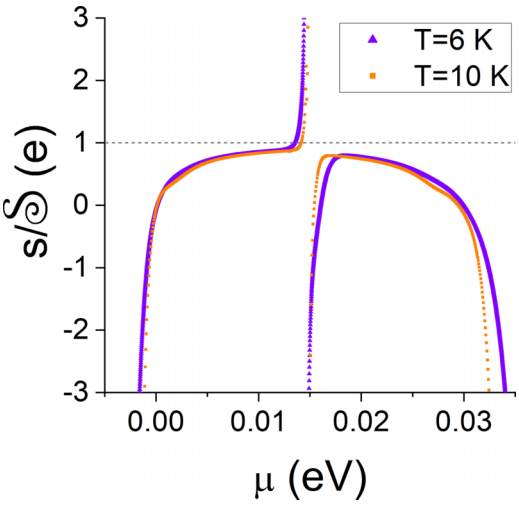

FIG. 9. Ratio $s/\mathcal{S}$ for zz1-$L8W12$ ribbon at $T = 6$ K and $T = 10$ K in units of the elementary charge e. Horizontal dashed gray line indicates a value of e.

Figure 8(b) shows the ratio $s(\mu)/\mathcal{S}(\mu)$ for the gap region highlighted in yellow in Fig. 8(a). The ratio presents an asymmetric line shape due to the asymmetry of both τ and D at the gap edges of the zz1-$L8W2$ ribbon; see Fig. 2(d). The ratio at $T = 10$ K grows from the valence gap edge near $\mu = 0$ reaching a constant value of $\sim e$ across the gap, except for a sharp discontinuity at midgap ($\mu_{\rm gmp} \simeq 0.055$ eV), and falls down near the conduction gap edge. At higher temperature, $T = 100$ K, the ratio $s/\mathcal{S}$ shows smoother variation and nearly constant e value over a smaller region.

The relation $\mathcal{S} \simeq s/e$ is also valid in the gap region of wider zz1 ribbons. Figure 9 shows the ratio $s/\mathcal{S}$ for the $L8W12$ ribbon at low T. As the band gap for this ribbon is $\simeq 0.027$ eV, an approximated constant ratio of e occurs within this gap value at $T = 6$ K and $T = 10$ K. For both T, the ratio exhibits a discontinuity near the gap midpoint $\mu_{\rm gmp} \simeq 0.014$ eV. The thermal quantities s and $\mathcal{S}$ at low T for this wider zz1-$L8W12$ system in Fig. 5(a) present similar behavior compared to the narrower zz1-$L8W2$ ribbon shown in Fig. 8. The main difference is that the band gap narrows for the wider $L8W12$ ribbon, and as a result, the interconnection between s and $\mathcal{S}$ signals, and their ratio $s/\mathcal{S}$, occurs over a smaller energy scale. Similar results for the ratio persist even at higher temperatures for the zz2-$L8W2$ system, as expected from the larger energy scales involved [35]. The equivalence between electronic transport and thermodynamic response, as given by $\mathcal{S} \simeq s/e$, suggests that $\mathcal{S}$ can be regarded as the transported entropy per unit charge in the gapped regime. The connection between these quantities could be explored and exploited in different materials.

IV. CONCLUSIONS

When graphene ribbons are asymmetrically doped along the zigzag edges a gap opens, and a flat band can remain for an undoped edge of the ribbon. The entropy per particle s is sensitive to the flat band, resulting in an antisymmetric (for pristine ribbons) and an asymmetric peak-dip curve whereas

the Seebeck signal $\mathcal{S}$ has a finite value of $\mathcal{S} = -2\frac{k_B}{e}\ln 2$ right at the flat-band energy for a one-doped-edge ribbon. s and $\mathcal{S}$ reach their highest amplitudes inside the gap with a dip-peak structure and fulfilling the relation $\mathcal{S} \simeq s/e$ all across the gap—except at midpoint for narrow and wide ribbons. This relation is especially clear at low temperatures, since at higher temperatures its dependence on chemical potential is blurred and softened. The Seebeck coefficient can then be seen as the transported entropy per charge within the gapped regime. The large magnitudes of s and $\mathcal{S}$ signals within transport gaps can be useful for band gap estimation [41], while the sign $\mathcal{S}$ is determined by the local band curvature. It would also be interesting to explore if the ratio $s/\mathcal{S}$ as function of chemical potential can indicate changes in the quasiparticle charge as materials may undergo transitions to strongly correlated regimes and possible charge fractionalization [42].

ACKNOWLEDGMENTS

N.C. acknowledges support from ANID Fondecyt Iniciación en Investigación Grant No. 11221088 and UTA, and the hospitality of Ohio University, P.V. acknowledges support from ANID Fondecyt Regular Grant No. 1210312 and ANID PIA/Basal Grant No. AFB220001, and S.E.U. acknowledges support from the U.S. Department of Energy, Office of Basic Energy Sciences, Materials Science and Engineering Division.

[1] The Faraday constant is the product of the elementary charge e and Avogadro number N_A, $F \equiv eN_A$.
[2] M. R. Peterson and B. S. Shastry, Phys. Rev. B **82**, 195105 (2010).
[3] T. W. Silk, I. Terasaki, T. Fujii, and A. J. Schofield, Phys. Rev. B **79**, 134527 (2009).
[4] V. Zlatić, R. Monnier, J. Freericks, and K. W. Becker, Phys. Rev. B **76**, 085122 (2007).
[5] J. Mravlje and A. Georges, Phys. Rev. Lett. **117**, 036401 (2016).
[6] The electronic entropy per particle s is also referred as differential entropy per particle. Through Maxwell relations, s can also be expressed as $s = (\frac{\partial S}{\partial N})_T = -(\frac{\partial \mu}{\partial T})_N = (\frac{\partial N}{\partial T})_\mu (\frac{\partial N}{\partial \mu})_T^{-1}$, with S the total electronic entropy and $N = \int_{-\infty}^{\infty} D(\varepsilon) f(\varepsilon, T, \mu) d\varepsilon$ the charge carrier number at thermal equilibrium.
[7] A. A. Varlamov, A. V. Kavokin, and Y. M. Galperin, Phys. Rev. B **93**, 155404 (2016).
[8] V. Y. Tsaran, A. Kavokin, S. Sharapov, A. Varlamov, and V. Gusynin, Sci. Rep. **7**, 10271 (2017).
[9] D. Grassano, O. Pulci, V. O. Shubnyi, S. G. Sharapov, V. P. Gusynin, A. V. Kavokin, and A. A. Varlamov, Phys. Rev. B **97**, 205442 (2018).
[10] V. Shubnyi, V. Gusynin, S. Sharapov, and A. Varlamov, Low Temp. Phys. **44**, 561 (2018).
[11] Y. Galperin, D. Grassano, V. Gusynin, A. Kavokin, O. Pulci, S. Sharapov, V. Shubnyi, and A. Varlamov, J. Exp. Theor. Phys. **127**, 958 (2018).
[12] I. Sukhenko, S. Sharapov, and V. Gusynin, Low Temp. Phys. **46**, 264 (2020).
[13] Y. Kulynych and D. O. Oriekhov, Phys. Rev. B **106**, 045115 (2022).
[14] Y. M. Zuev, W. Chang, and P. Kim, Phys. Rev. Lett. **102**, 096807 (2009).
[15] L. Hao and T. K. Lee, Phys. Rev. B **81**, 165445 (2010).
[16] C.-R. Wang, W.-S. Lu, L. Hao, W.-L. Lee, T.-K. Lee, F. Lin, I.-Chun Cheng, and J.-Z. Chen, Phys. Rev. Lett. **107**, 186602 (2011).
[17] F. Mazzamuto, V. H. Nguyen, Y. Apertet, C. Caër, C. Chassat, J. Saint-Martin, and P. Dollfus, Phys. Rev. B **83**, 235426 (2011).
[18] M. S. Hossain, D. H. Huynh, P. D. Nguyen, L. Jiang, T. C. Nguyen, F. Al-Dirini, F. M. Hossain, and E. Skafidas, J. Appl. Phys. **119**, 125106 (2016).
[19] N. Hartman, C. Olsen, S. Lüscher, M. Samani, S. Fallahi, G. C. Gardner, M. Manfra, and J. Folk, Nat. Phys. **14**, 1083 (2018).
[20] A. Rozen, J. M. Park, U. Zondiner, Y. Cao, D. Rodan-Legrain, T. Taniguchi, K. Watanabe, Y. Oreg, A. Stern, E. Berg *et al.*, Nature (London) **592**, 214 (2021).
[21] Y. Saito, F. Yang, J. Ge, X. Liu, T. Taniguchi, K. Watanabe, J. Li, E. Berg, and A. F. Young, Nature (London) **592**, 220 (2021).
[22] Y. H. Kim, H. J. Lee, and S.-R. Eric Yang, Phys. Rev. B **103**, 115151 (2021).
[23] C. C. Rinzler and A. Allanore, Philos. Mag. **96**, 3041 (2016).
[24] N. Pérez, C. Wolf, A. Kunzmann, J. Freudenberger, M. Krautz, B. Weise, K. Nielsch, and G. Schierning, Entropy **22**, 244 (2020).
[25] A. Y. Kuntsevich, Y. Tupikov, V. Pudalov, and I. Burmistrov, Nat. Commun. **6**, 7298 (2015).
[26] M. Fujita, K. Wakabayashi, K. Nakada, and K. Kusakabe, J. Phys. Soc. Jpn. **65**, 1920 (1996).
[27] K. Nakada, M. Fujita, G. Dresselhaus, and M. S. Dresselhaus, Phys. Rev. B **54**, 17954 (1996).
[28] D. Gunlycke, J. Li, J. Mintmire, and C. White, Appl. Phys. Lett. **91**, 112108 (2007).
[29] H. S. Moon, J. M. Yun, K. H. Kim, S. S. Jang, and S. G. Lee, RSC Adv. **6**, 39587 (2016).
[30] Armchair graphene ribbons are naturally gapped, and doping does not qualitatively change their gapped states.
[31] A. L. Rockwood, Phys. Rev. A **30**, 2843 (1984).
[32] D. Moldovan, M. Andelković, and F. Peeters, PYBINDING ver. 0.9.5: A PYTHON package for tight-binding calculations.
[33] C. W. Groth, M. Wimmer, A. R. Akhmerov, and X. Waintal, New J. Phys. **16**, 063065 (2014).
[34] P. Dollfus, V. H. Nguyen, and J. Saint-Martin, J. Phys.: Condens. Matter **27**, 133204 (2015).
[35] See Supplemental Material at http://link.aps.org/supplemental/10.1103/PhysRevB.107.075433 for a more complete description of pristine ribbons, wave functions in real space, analytical approximations for s and $\mathcal{S}$, results for high-temperature zz1 systems, and the ratio $s/\mathcal{S}$ for a zz2 system.
[36] Y.-W. Son, M. L. Cohen, and S. G. Louie, Phys. Rev. Lett. **97**, 216803 (2006).
[37] A. M. Alsharari, M. M. Asmar, and S. E. Ulloa, Phys. Rev. B **94**, 241106(R) (2016).

[38] H. Feldner, Z. Y. Meng, T. C. Lang, F. F. Assaad, S. Wessel, and A. Honecker, Phys. Rev. Lett. **106**, 226401 (2011).

[39] Magnetic order on the edges may induce additional quasiparticles as magnons, affecting the similarity of s and $\mathcal{S}$ responses seen at low temperatures for the electronic degree of freedom.

[40] The total electronic entropy S in a twisted bilayer graphene moiré unit cell is $S \sim k_B \ln 2$ [20]. A similar value for S is obtained from quantum dot conductance measurements, indicating a twofold degenerate state [19].

[41] H. Goldsmid and J. Sharp, J. Electron. Mater. **28**, 869 (1999).

[42] T. Senthil and O. Motrunich, Phys. Rev. B **66**, 205104 (2002).